Optics Letters

Visualizing surface plasmon polaritons by their gradient force

Junghoon Jahng,[1] Faezeh Tork Ladani,[2] Ryan Muhammad Khan,[3] Xiaowei Li,[3] Eun Seong Lee,[4] and Eric Olaf Potma[2,3,*]

[1]Department of Physics and Astronomy, University of California, Irvine, California 92697, USA
[2]Department of Electrical Engineering and Computer Science, University of California, Irvine, California 92697, USA
[3]Department of Chemistry, University of California, Irvine, California 92697, USA
[4]Center for Nanometrology, Korea Research Institute of Standards and Science, 267 Gajeong-ro, Yuseong-gu, Daejeon 304-340, South Korea
*Corresponding author: epotma@uci.edu

Received 11 September 2015; revised 29 September 2015; accepted 7 October 2015; posted 7 October 2015 (Doc. ID 249851); published 28 October 2015

A new method is presented for visualizing the electric field distributions associated with propagating surface-plasmon-polariton (SPP) modes directly in the near-field. The method is based on detecting the photo-induced gradient force exerted by the evanescent field onto a sharp and polarizable tip. Using a photo-induced force microscope (PiFM), images of propagating SPPs are obtained on flat gold surfaces.

OCIS codes: (240.6680) Surface plasmons; (240.5420) Polaritons; (180.4243) Near-field microscopy.

http://dx.doi.org/10.1364/OL.40.005058

Surface plasmon polaritons (SPPs) are propagating surface plasmon modes, which have become relevant as carriers of electromagnetic information in photonic devices [1]. The electric field distribution associated with the SPP mode is manifest in the near-field only, and to visualize the mode requires a near-field interaction that produces a detectable signal. Popular methods to probe SPPs rely on coupling information from the near-field to the far-field, such as detecting the leakage radiation with a far-field photodetector [2], near-field coupling to a waveguide [3], or using subwavelength optical antennae to scatter near-field information to the far-field.

The aforementioned methods for probing SPPs are all based on detecting an optical signal. The SPP modes can also be visualized with nonoptical detection methods; an example includes electric field mapping based on photon-emission electron microscopy [4]. In this example, electrons are ejected in the near-field and detected by a far-field electron detector. In this Letter, we report a new nonoptical approach for imaging SPP excitations on flat surfaces. Our method is based on detecting the force exerted by the surface electric field on the polarizable apex of a cantilevered tip. Unlike most approaches, the force is inherently detected in the near-field, without the need to transfer information to a far-field detector.

It is well known that polarizable objects subjected to the steep gradients of surface plasmon modes can experience sizable forces. Such forces have previously been described [5], and have, for instance, been used in applications that involve optical tweezers [6,7]. Forces associated with plasmon modes have also been proposed for their utility in various forms of scan probe microscopy [8,9]. Here we use the gradient force that is exerted on an atomic force microscopy (AFM) tip as a probe for detecting the electric component of the SPP surface field. This can be accomplished with the photo-induced force microscopy (PiFM) technique, an approach for generating force maps that has previously been developed for visualizing molecules at the nanoscale [10–13]. Recently, the PiFM technique was used to map the electric field distribution of freely propagating light in the focal plane of a high numerical aperture lens [14]. The photo-induced force can also be used to map purely evanescent fields, as recently suggested for the measurement of a localized surface plasmon on a bowtie antenna [15]. However, localized surface plasmons in nanoscopic gaps are a challenge to measure with a tip, as the tip may alter the gap mode. Questions remain about the origin of the detected force in the immediate vicinity of the gap, as thermal artifacts may govern the mechanical response of the cantilever. Here, we focus on the evanescent fields associated with propagating SPP modes, for which surface fields are well described by analytical expressions, and show that the electric field can be mapped through the gradient force in a clean and artifact-free manner.

A schematic of our measurement is given in Fig. 1, depicting an interface between three media, labeled as 1, m, and 2, which are characterized by their permittivity $\varepsilon_{1,m,2}$ and permeability $\mu_{1,m,2}$. The interface is illuminated with light of wave vector k_1 in the lower medium 1 at an angle θ_1. If the medium m is a thin metal film, beyond the critical angle, an evanescent field is generated at the interface between medium m and medium 2 with amplitudes E_i polarized along $i = x, y, z$. A tip with a (isotropic) polarizability $\alpha = \alpha' + j\alpha''$ is placed in the upper medium 2 and allowed to interact with the components of the evanescent field, inducing a dipole $p_i = \alpha E_i$ at the apex.

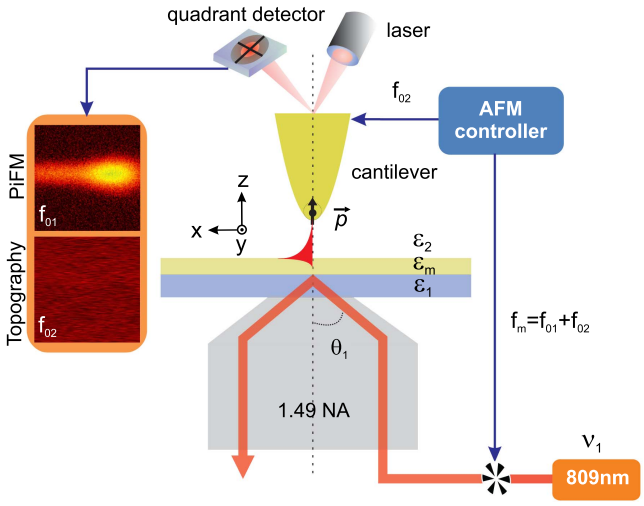

Fig. 1. Schematic of the setup for measuring the electric field of a propagating SPP mode at a gold/air interface.

The time-averaged force that is exerted on the tip by the field is written as [16]

$$\langle F(t)\rangle = \frac{1}{2}\sum_i \mathrm{Re}\{p_i^* \nabla E_i\}. \quad (1)$$

In the case of p-polarized incident fields with amplitude E_0^p, the photo-induced force contains components along the $\hat{x}$ and $\hat{z}$ directions as follows:

$$\langle F^p(t)\rangle = \frac{1}{2}|A^p|^2[\alpha'' k_1 \sin\theta_1 \hat{x} - \alpha' \gamma \hat{z}], \quad (2)$$

where γ is related to the decay length of the evanescent field along $\hat{z}$, and A^p is given as

$$A^p = E_0^p t^p(\theta_1)\left\{2\frac{\varepsilon_1\mu_1}{\varepsilon_2\mu_2}\sin^2\theta_1 - 1\right\}^{1/2} e^{-\gamma z}. \quad (3)$$

Here, $t^p(\theta_1)$ is the Fresnel transmission coefficient for the three-layered medium with p-polarized light, and $\mu_{1,2}$ are the permeabilities for media 1 and 2, respectively. Note that in this simple model, multiple scattering effects that describe coupling between the tip and interface are not considered.

Equation (2) shows two force components. The component directed along $\hat{x}$ scales with the imaginary part of α and originates from the scattering force. The force component along $\hat{z}$ is proportional to the real part of α and stems from the gradient force. Hence, in this configuration, the force components from the gradient and scattering force are projected in orthogonal directions. Because the cantilever-based measurement is most sensitive to forces directed along the $\hat{z}$ direction, the detected force is dictated by the *gradient force* in the configuration considered here. In this fashion, p-polarized evanescent fields can be probed directly in the near field by registering the photo-induced gradient force exerted on the tip.

SPP modes at the gold/air interface are excited when the p-polarized evanescent field of optical frequency ω is momentum matched to the propagating surface field with wave vector $k_{spp} \approx (\omega/c)\{\varepsilon_m(\omega)/[\varepsilon_m(\omega)+1]\}^{1/2}$. Under these conditions achieved at the surface plasmon coupling angle θ_{sp}, the dominant evanescent field contributions result from the surface plasmon excitation, and the measured gradient force becomes an effective probe for the SPP mode.

Our experimental setup consists of a custom-modified atomic force microscope (VistaScope, Molecular Vista Inc.) configured for PiFM measurements [12]. The inverted microscope system is outfitted with an NA = 1.49 oil-immersion objective, a sample stage scanner, an AFM scan head, and transmission and reflection optics for sample inspection. The incident beam, derived from a 200 fs Ti:sapphire laser (MaiTai, Spectra-Physics), is linearly polarized and passed through an aperture to generate a narrow pencil beam (<1 mm in diameter) at the back aperture of the objective lens. The position of the laser beam at the back aperture plane is adjusted with a linear translation stage for precise control of the incident angle θ_1. In this configuration, the microscope objective transforms the input beam into a focal spot of diameter ~3 μm at the sample [17]. In this study, we use 30 nm gold films deposited on 0.17 mm thick borosilicate coverslips. The average power of the 809 nm incident laser beam, measured at the back aperture plane, is 0.40 mW. Using an acoustic optic modulator, the laser light is amplitude modulated at a frequency f_m, as specified below.

We use a 30 nm radius gold-coated silicon tip (ACTGG, AppNano) as the probe. The implemented cantilever system exhibits a first mechanical resonance at frequency $f_{01} = 247.4$ kHz with a spring constant $k_1 = 37$ N/m and quality factor $Q_1 = 543$. A second mechanical resonance is found at $f_{02} = 1564.6$ kHz with $k_2 = 1479.82$ N/m and $Q_2 = 697$. Theoretically, the minimum detectable forces of each cantilever eigenmode can be computed as $F_{\min_i} = \sqrt{4k_i k_B T B/Q_i\omega_{0i}}$ [18,19], where B is the measurement bandwidth and i is ith eigenmode. For the fundamental resonance with $B = 10$ Hz and $T = 300$ K, the minimum detectable force in the absence of external noise sources is estimated as 8.52×10^{-14} N. In our measurements, performed under ambient temperature and pressure, the noise floor is determined by the electrical measurement noise and the thermal noise and is found at 1.26×10^{-13} N.

The multiple eigenmodes of the cantilever can be used for measuring both the topography and the PiFM signal. In common AFM measurements, the first mechanical resonance is typically chosen to probe the sample's topography. However, in principle, other eigenmodes of the cantilever can be used for AFM measurements as well [20]. In this work, the topographic measurements are carried out at the second resonance at f_{02}, which, compared with the first resonance, has a higher stiffness suitable for maintaining a small oscillation amplitude at a stable tip-sample distance. The cantilever is actively driven at f_{02} with an oscillation amplitude of $A_2 = 15$ nm, and the average tip-interface distance is set at 56 nm. The PiFM signal is obtained in the sideband coupling mode and detected at the first mechanical resonance at f_{01}. For this purpose, the laser beam is amplitude modulated at a frequency of $f_m = f_{01} + f_{02}$ with an acoustic optic modulator. Under these conditions, the detected force is demodulated at $f_m - f_{02}$, which overlaps with the first mechanical resonance of the cantilever [10]. The sideband coupling mode is chosen because it is sensitive to the gradient force while contributions from the scattering force are suppressed.

As shown in Fig. 1, the system acquires PiFM (f_{01} channel) and topography images (f_{02} channel) simultaneously. For the

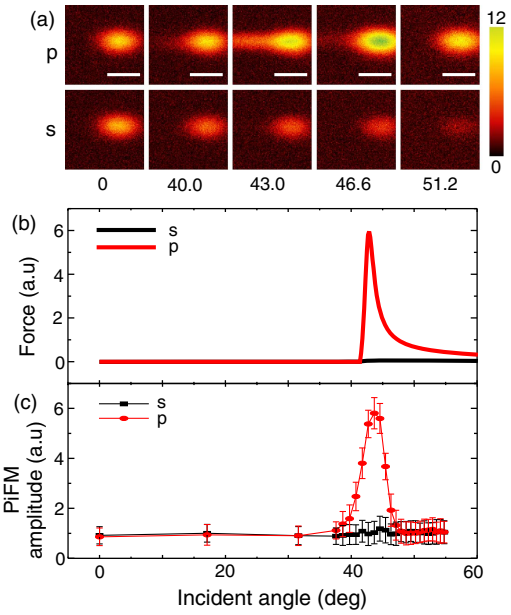

Fig. 2. Force amplitude in the near-field as a function of the incident illumination angle. (a) PiFM images near the illumination spot for various incident angles. The scale bar is 5 μm. (b) Calculated force exerted by the SPP excitation based on Eq. (2). The force is shown for both p polarization (red) and s polarization (black) of the incident light. (c) Measured PiFM amplitude when the tip is placed in the tail of the propagating SPP mode.

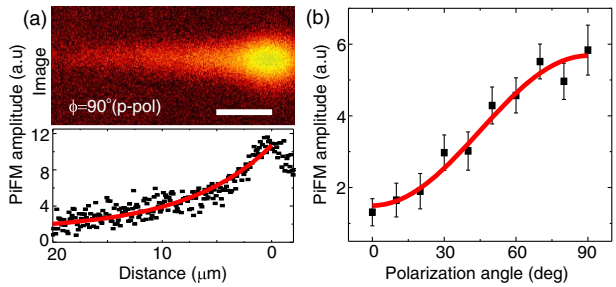

Fig. 3. (a) PiFM image for $\phi = 90^o$ (upper panel) and 1D cross section along the propagation direction (lower panel). The red line is an exponential fit with a $1/e$ value of 7.83 μm. (b) SPPs intensity with respect to ϕ, measured 6 μm from the center of the illumination spot. The scale bar is 5 μm. The black dots denote the measured PiFM signal, and the red line is a fit with the function $\sin^2\phi$.

flat gold films studied here, no significant features are expected in the topography image. Optical artifacts in the topography channel, due to light-induced changes in the tip-sample distance, are kept below the noise. In the PiFM channel, on the other hand, clear photo-induced forces on the order of 10 pN are observed upon illumination.

Figure 2(a) shows PiFM images recorded in the vicinity of the focal spot for different incident angles θ_1. The bright spot indicates that the tip experiences an optically induced force when scanned across the focus. A detectable force is seen for both p and s polarization of the laser beam with almost equal magnitude for small incident angles, as shown here for $\theta_1 = 0$. For larger θ_1, however, the measured photo-induced force differs markedly for different input polarizations. Close to θ_{sp}, near 43°, the force induced by p-polarized light grows stronger, whereas the force amplitude measured for s-polarized fields remains weak. In addition, a propagating tail, in the direction of the SPP wave vector, is seen emanating from the focal spot for p-polarized light. This tail is not observed when the polarization state of the laser beam is changed to s. For larger angles beyond 43°, the measured photo-induced force decreases for both input polarizations.

We attribute the observed tail to the excitation of the SPP mode, which, based on momentum matching, is expected under the examined conditions for $\theta_1 = 42.84°$. Figure 2(b) shows the calculated force based on Eq. (2) as a function of θ_1, assuming a tip-sample distance of 56 nm. The increase in the photo-induced force beyond the critical angle is predicted only for p-polarized light, as expected for the excitation of the SPP mode. This polarization-selective behavior is reproduced in the experiment. In Fig. 2(c) the measured force amplitude is plotted as a function of incident angle. In this measurement, the force was determined in the propagation tail 6 μm away from the center of the focal spot. The maximum force at this location is found at 43°, close to the expected θ_{sp} of the SPP mode. The shape of the experimental curve lacks the sharp offset near θ_{sp} seen in the calculation, which we attribute to the limited angular resolution of the experiment, determined by the angular width of the focused pencil beam (~2.5°).

To investigate the SPP-induced component to the force signal further, we mapped the spatial distribution of the mode away from the launching spot. Figure 3(a) shows a PiFM image of the SPP mode excited with p-polarized light at the SPP coupling angle. The image reveals that the intensity decays along the propagation direction in an exponential matter, with a fitted $1/e$ value of 7.83 μm. We note that away from the central spot, no field contributions from the original light field are expected, and, thus, the surface field solely results from the SPP mode. Therefore, these measurements demonstrate that PiFM is capable of registering electric field distributions in the near-field, such as those associated with SPP excitations.

The exponential decay of the measured photo-induced force in the direction of propagation mimics the exponential decay of a propagating SPP mode subject to dissipative losses. The predicted propagation length of the SPP mode at 809 nm, using ε_m of a 30 nm gold film, is 7.54 μm [16,21], which corroborates the distances observed in the PiFM measurements presented here.

As the polarization angle ϕ is changed, the relative component of p-polarized light changes as well. When $\phi = 90°$, the input light is purely p polarized, whereas at $\phi = 0°$, the incident beam is s polarized. In Fig. 3(b), the magnitude of photo-induced force is given as a function of the polarization angle ϕ. If it is assumed that the detected force is proportional to the modulus square of the SPP surface field, as in Eq. (2), we expect that the force follows a $\sin^2\phi$ dependence. The red curve in Fig 3(b) is a fit to the $\sin^2\phi$ function, indicating that the measured force is approximately linearly proportional to the intensity of the SPP field.

Note that the measurements were obtained in noncontact scanning mode of the tip, in which the tip never touches the gold film. In this configuration, the system is expected to be

insensitive to thermal expansion artifacts, which are estimated to affect the tip-sample distance by less than 10 pm in our measurements [22]. Measuring the thermal expansion would require tip-sample distances in the pm range, which is orders of magnitude smaller than the shortest dynamic tip-sample distances in our measurements. Therefore, the detected force is attributed to a purely electromagnetic force, the gradient force, as described in Eq. (2). Under the conditions examined here, the PiFM images resemble intensity maps of the SPP mode with the correct decay length and polarization dependence. These observations can be satisfactorily explained by the simple model used here, indicating that electromagnetic coupling between the tip and sample is relatively small at tip-sample distances of 50 nm or more. Nonetheless, if the experiments are carried out at shorter tip-sample distances, coupling between tip and sample is expected to become important, and a more complete modeling of the fields in the junction would be appropriate for such cases.

The results discussed here clearly show that the PiFM technique is capable of mapping propagating SPP modes on flat surfaces. Our analysis shows that PiFM is sensitive to the gradient force exerted on the tip by the electric component of the evanescent SPP field. The PiFM approach for mapping surface fields is complementary to near-field optical detection techniques, although it is based on a fundamentally different detection strategy. One of the merits of the force detection method compared to optical scattering near-field techniques is its insensitivity to far-field interference effects. Besides the mapping of SPP modes on flat metal surfaces, the PiFM method is also promising for the real space visualization of other propagating surface modes, such as plasmons in graphene and the evanescent fields of semiconductor waveguides. In addition, the force detection approach may prove useful for imaging of localized surface modes. As a scan-probe technique, PiFM features a high spatial resolution, which can reach 10 nm or less in tapping mode [11,12]. Combined with the high resolution topographic contrast readily available through the AFM detection channel, the PiFM technique may grow into a practical near-field tool for mapping localized surface fields on nanoscopic devices such as nano-antennae and photonic crystal resonators.

Funding. National Science Foundation (NSF) (1414466).

REFERENCES

1. J. Homola, S. S. Yee, and G. Gauglitz, Sens. Actuators B **54**, 3 (1999).
2. B. Hecht, H. Bielefeldt, L. Novotny, Y. Inouye, and D. W. Pohl, Phys. Rev. Lett. **77**, 1889 (1996).
3. R. Zia, J. A. Schuller, and M. L. Brongersma, Phys. Rev. B **74**, 165415 (2006).
4. A. Kubo, N. Pontius, and H. Petek, Nano Lett. **7**, 470 (2007).
5. J. R. Arias-González and M. Nieto-Vesperinas, J. Opt. Soc. Am. A **20**, 1201 (2003).
6. M. Righini, A. S. Zelenina, C. Girard, and R. Quidant, Nat. Phys. **3**, 477 (2007).
7. M. L. Juan, M. Righini, and R. Quidant, Nat. Photonics **5**, 349 (2011).
8. F. De Angelis, G. Das, P. Candeloro, M. Patrini, M. Galli, A. Bek, M. Lazzarino, I. Maksymov, C. Liberale, L. C. Andreani, and E. Di Fabrizio, Nat. Nanotechnol. **5**, 67 (2010).
9. F. De Angelis, R. P. Zaccaria, and E. Di Fabrizio, Opt. Express **20**, 29629 (2012).
10. I. Rajapaksa, K. Uenal, and H. K. Wickramasinghe, Appl. Phys. Lett. **97**, 073121 (2010).
11. I. Rajapaksa, K. Uenal, and H. K. Wickramasinghe, Appl. Phys. Lett. **99**, 161103 (2011).
12. J. Jahng, J. Brocious, D. A. Fishman, F. Huang, X. Li, V. A. Tamma, H. K. Wickramasinghe, and E. O. Potma, Phys. Rev. B **90**, 155417 (2014).
13. J. Jahng, J. Brocious, D. A. Fishman, S. Yampolsky, D. Nowak, F. Huang, V. A. Apkarian, H. K. Wickramasinghe, and E. O. Potma, Appl. Phys. Lett. **106**, 083113 (2015).
14. F. Huang, V. A. Tamma, Z. Mardy, J. Burdett, and H. K. Wickramasinghe, Sci. Rep. **5**, 10610 (2015).
15. J. Kohoutek, D. Det, A. Bonakdar, R. Gelfand, A. Sklar, O. G. Memis, and H. Mohseni, Nano Lett. **11**, 3378 (2011).
16. L. Novotny and B. Hecht, *Principles of Nano-Optics* (Cambridge, 2006).
17. X. Liu, Y. Wang, and E. O. Potma, Opt. Lett. **36**, 2348 (2011).
18. Y. Martin, C. C. Williams, and H. K. Wickramasinghe, J. Appl. Phys. **61**, 4723 (1987).
19. T. D. Stowe, K. Yasumura, T. W. Kenny, D. Botkin, K. Wago, and D. Rugar, Appl. Phys. Lett. **71**, 288 (1997).
20. R. Garcia and E. T. Herruzo, Nat. Nanotechnol. **7**, 217 (2012).
21. R. Viter, Z. Balevicius, A. Abou Chaaya, I. Baleviciute, S. Tumenas, L. Mikoliunaite, A. Ramanavicius, Z. Gertnere, A. Zalesska, V. Vataman, V. Smyntyna, D. Erts, P. Miele, and M. Bechelany, J. Mater. Chem. C **3**, 6815 (2015).
22. F. Lu, M. Jin, and M. A. Belkin, Nat. Photonics **8**, 307 (2014).